Applied Catalysis B: Environmental 196 (2016) 142–154

Contents lists available at ScienceDirect

Applied Catalysis B: Environmental

journal homepage: www.elsevier.com/locate/apcatb

Insight into the mechanism of catalytic combustion of acrylonitrile over Cu-doped perovskites by an experimental and theoretical study

Runduo Zhang*, Peixin Li, Ran Xiao, Ning Liu, Biaohua Chen

State Key Laboratory of Chemical Resource Engineering, Beijing University of Chemical Technology, Beijing 100029, PR China

ARTICLE INFO

Article history:
Received 9 February 2016
Received in revised form 11 April 2016
Accepted 15 May 2016
Available online 16 May 2016

Keywords:
Acrylonitrile
Selective catalytic combustion
Perovskite
Cu substitution

ABSTRACT

A series of $LaFeO_3$, $La_2Cu_2O_4$, and Cu-doped perovskite-typed $LaB_{0.8}Cu_{0.2}O_3$ (B = Fe, Co, and Mn) catalysts were studied for the selective catalytic combustion of acrylonitrile (C_2H_3CN). The physicochemical properties of these materials were characterized by XRD, N_2 sorption, H_2-TPR, and XPS, thereafter correlating to their diverse evolutions of N_2 yield. The best performance was achieved over the $LaFe_{0.8}Cu_{0.2}O_3$ sample owing to an easy transformation from Cu^{2+} to Cu^0 at low temperatures. Moreover, the mechanism on selective catalytic combustion of acrylonitrile over $LaFeO_3$ and $LaFe_{0.8}Cu_{0.2}O_3$ was investigated by *in-situ* DRIFTs and density functional theory (DFT) calculations. It has been noted that malonic acid species were generated on the surface of $LaFe_{0.8}Cu_{0.2}O_3$ sample and the acrylic species steadily existed over $LaFeO_3$, indicating that the strongly oxidative copper ion promotes an oxidation of C-terminal to carboxylic acid species at low temperatures. In addition, the copper substitution into $LaFeO_3$ can greatly reduce energy barrier for the transformation from —NH—O to —N—OH, which is thought as the rate-determining step for N_2 formation. In summary, the catalytic combustion of acrylonitrile commonly follows an oxidation-dominate mechanism over $LaFe_{0.8}Cu_{0.2}O_3$, whereas fulfills with a hydrolysis-dominate mechanism over $LaFeO_3$. 5% H_2O addition into the feed caused a slightly and reversible decrease in N_2 yield as well as an improved NO production, while a poisoning by 100 ppm SO_2 was found due to serious coverage of active centers by sulfurous species.

1. Introduction

The purification of nitrile emissions coming from acrylonitrile (CH_2=CH—C≡N) production becomes more and more urgent and significant due to its intensively carcinogenic properties which lead to serious environmental and human health problems. Incineration is a simple method to remove this nitrile gas, but the related process is normally operated at high temperatures (around 800 °C), which needs additional fuel consumption. More importantly, direct incineration might lead to the formation of a large number of byproduct such as nitrogen oxides (NO_x), which causes a secondary pollution. Conversely, catalytic combustion of acrylonitrile has been widely studied owing to the relatively lower operation temperature and its excellent performances especially high N_2 and CO_2 selectivity. Therefore, exploring the effective catalytic material which has good catalytic activity for acrylonitrile removal and high selectivity of the targeted products (N_2 and CO_2) is particularly necessary. Gervasini et al. studied that the synergic effects of Ba—CuO—Cr_2O_3/Al_2O_3 catalyst associated with ozone which was used as strong oxidant during acrylonitrile combustion [1]. However, this work only focused on the acrylonitrile conversion but ignored the N_2 selectivity. Nanba et al. [2,3] demonstrated Ag was an efficient catalyst for acrylonitrile decomposition and explored the effect of different support materials as well as indentified the oxidation state of Ag. Besides, zeolite-supported transition-metals were also reported to show excellent performances for nitrile combustion [4–7]. Cu-ZSM-5 completely converted acrylonitrile with an N_2 selectivity of 80% or more at >350 °C. The redox property between Cu^{2+} and Cu^+ is reported to be responsible for combustion activity [6,7]. In addition, Poignant et al. [8] proposed a mechanism that acrylonitrile adsorbed on Cu^+ decomposed rapidly into ethylene and cyanide (Cu^+CN) during the selective catalytic reduction of NO_x by propane. Anyhow, Cu species over zeolites could effectively promote the decomposition activity of acrylonitrile and improve N_2 selectivity at a relatively low temperature. However, few manuscripts, involving selective catalytic combustion of nitrile by the mixed oxides, especially perovskite-type oxides with their unique structure and versatility of compositions, have been reported in recent years.

Perovskites are described by a general ABO_3 formula, which have been proposed to be potential substitutes of noble metals

* Corresponding author.
E-mail address: zhangrd@mail.buct.edu.cn (R. Zhang).

http://dx.doi.org/10.1016/j.apcatb.2016.05.025
0926-3373/

being a redox catalyst [9]. In the perovskite structure, A cation can be a lanthanide or alkaline-earth cation, while B cation is a transition-metal element which is commonly believed to serve as the active sites in environmental catalytic reaction [10,11]. These materials commonly show satisfactory activities not only in the complete oxidation system such as CO [12,13], CH_4 [14], VOCs [15,16] *etc.*, but also in the selective catalytic reduction (SCR) of NO system. Diverse reductants such as C_3H_6 [17–20] and NH_3 [21] were applied for the NO-SCR processes. Both Zhang [20] and Yang [22] have demonstrated that SCR performance along with N_2 selectivity is improved by an incorporation of Cu^{2+} into the lattice of perovskites. In the process of mechanism research, some important intermediates such as —CN and adsorbed $(CN)_2$ yielding during the SCR of NO are also the initial *ad*species during the catalytic combustion of acrylonitrile [22]. A similar result that acrylonitrile has been regarded as a possible intermediate to form N_2 was also studied by Nanba et al. [8]. Therefore, there is reason to think that these perovskite-type materials, especially doped by Cu^{2+}, would show promising performances in the catalytic combustion of acrylonitrile. Aiming at developing an industrial catalyst, special attention should be paid for the influence of steam on catalytic performance because large amount of water vapor would be generated during this combustion process. The resistance towards SO_2 poisoning also needs to be considered although acrylonitrile production generally belongs to a low-contamination process.

In the present study, $LaB_{0.8}Cu_{0.2}O_3$ (B═Fe, Co, and Mn) was synthesized by citrate complexation procedure and further characterized by N_2 physisorption, X-ray diffraction (XRD), H_2-temperature programmed reduction (TPR) and X-ray spectroscopy (XPS). *In-situ* diffuse reflectance infrared Fourier transform spectroscopy (DRIFTS) was performed for a better understanding of reaction mechanism for acrylonitrile catalytic combustion occurring over $LaFeO_3$ and $LaFe_{0.8}Cu_{0.2}O_3$ as well as how the Cu^{2+} ions promote activity of acrylonitrile elimination and improve N_2 selectivity. The reaction paths of acrylonitrile oxidation, including the free energy of intermediates and transition states, were analyzed by density functional theory (DFT) calculations in order to clarify the details of bond formation and fracture of the corresponding intermediates species. Ultimately, a deep insight into mechanism of catalytic combustion of acrylonitrile to generate N_2 and CO_2, combining *in-situ* DRIFTs investigations with DFT calculations, over Fe-based perovskite doped by Cu^{2+} was herein represented. The influence of water vapor and sulfur dioxide on combustion performances was also addressed.

2. Experimental

2.1. Catalyst preparation

A series of perovskite catalysts with different B-site cations (B═Fe, Co, and Mn) partially substituted by Cu^{2+} was synthesized by the classical citrate complexation [21,23] (see details in Section S1 of Catalysts preparation in SI).

2.2. Characterization

These perovskite catalysts were characterized by several techniques including XRD, N_2 sorption, H_2-TPR, and XPS, with details being addressed in Section S2 of Characterization in SI.

2.3. Catalytic activity measurements

The catalytic combustion of acrylonitrile was performed in a quartz fixed-bed reactor (i.d. = 0.6 cm, L = 40 cm) under an atmosphere of 3000 ppm acrylonitrile and 1.6 vol% O_2, balanced by He with a space velocity of approximate 120,000 h^{-1}. The whole reaction pipeline was thermally insulated at 100 °C with heating tape. The water and sulfur resistance tests were also performed in a quartz fixed-bed reactor with H_2O and SO_2 being simultaneously introduced under space velocity of about 120,000 h^{-1}. The experimental facilities are described in Section S3 of Catalytic activity measurements in SI.

2.4. In-situ *DRIFTS study*

In-situ diffuse reflectance infrared Fourier-transform spectroscopy (DRIFTS) was performed to investigate the surface absorbed species upon temperature. The concentrations of acrylonitrile and O_2 in the gas mixture were 1.2 vol% and 6.4 vol%, respectively, with He as the balance gas, and the total flow rate was 60 ml/min. The *in-situ* DRIFTS equipment and experimental method are presented in Section S4 of *In-situ* DRIFTS study in SI.

2.5. Computational methods

All of the calculations were performed with the density functional theory (DFT) provided by the program DMol3 package [24]. Spin-polarized calculations were employed using the generalized gradient approximation (GGA) with the Perdew-Burke-Ernzerhof (PBE) method to describe the exchange and correlation energy in all calculations. For calculations of geometry optimization, a $1 \times 3 \times 1$ Mon-Khorst-Pack k-point mesh for the Brillouin zone sampling was used. Using periodic boundary, a plane-wave cutoff energy of 400 eV has been employed throughout. The $LaFeO_3$ crystal with an orthorhombic perovskite structure [*Pnma* (62)] was calculated with 28 atoms in the unit cell. We explore both possibilities using a supercell ($1 \times 2 \times 1$), slab model of the $LaFeO_3$ and $LaFe_{1-x}Cu_xO_3$ perovskite terminated upon the most common, (0 1 0) facet of the material [25,26].

The energy of adsorption, E_{ads}, for the acrylonitrile molecules on the surface is defined as:

$$E_{ads} = E_{adsorbate+surface} - E_{surface} - E_{gas}$$

where $E_{surface}$ is the total clean relaxation energy of the surface slab, E_{gas} is the energy of the gas-phase adsorbate, and $E_{adsorbate+surface}$ is the total energy of the composite system. Since the calculations are performed at 0 K and fixed cell volume, the differences in Gibbs free energy should equal the differences in total energy. By this definition, a negative value of E_{ads} corresponds to an exothermic and spontaneous adsorption process.

To locate saddle points and calculate the reaction pathway, the climbing image-the nudged elastic band (CI-NEB) method was used [27]. This is a "chain of states" method, where several intermediate states or images of the system are connected by springs to map out a reaction pathway between the initial and final states.

3. Results and discussion

3.1. Physicochemical properties

XRD patterns of the perovskite-type materials ($LaFeO_3$, $LaFe_{0.8}Cu_{0.2}O_3$, $LaCo_{0.8}Cu_{0.2}O_3$, $LaMn_{0.8}Cu_{0.2}O_3$, and La_2CuO_4) are illustrated in Fig. S1. All five as-prepared samples show pure perovskite structure, but the locations of diffraction peaks of these perovskite-type samples are slightly different, which result from the distinction of B-site metals. Furthermore, no diffraction line corresponding to external CuO or Cu_2O can be detected, suggesting that Cu is successfully incorporated into the perovskite lattice. Moreover, specific surface area (15–40 m^2/g) determined by N_2

sorption and crystallite size (10–25 nm) calculated by Scherrer equation, are listed in Table S1.

H_2-TPR profiles for different perovskites with and without Cu-doping are shown in Fig. S2, which is mainly used to investigate the influence of Cu substitution on the related redox abilities. The location and assignment of reduction peaks of as-prepared samples were detailedly discussed in Section S6 of Redox properties in SI. Seeing from Fig. S2, a large peak at 292 °C appearing in the case of La_2CuO_4 can be attributed to the reduction of Cu^{2+} to Cu^0, whereas a small peak at 546 °C may be possibly ascribed to the reduction of bulk CuO to Cu^0 [28]. There is no obvious reduction peak observed for $LaFeO_3$ in comparison with La_2CuO_4, indicating the limited redox ability of the former. Actually, $LaFeO_3$ was verified to be hardly reducible up to 700 °C [22,29]. The quantitative calculation of H_2 consumption and cation reduction percentage are described in Table S2. For all the Cu-doped samples, Cu being incorporated into the lattice of perovskites not only improved the redox ability at low temperatures but also facilitated the corresponding reduction percentages, for Co^{3+} from 73.0% to 98.6%, for Mn^{2+} from 66.7% to 79.2%, and for Fe^{3+} from 4.0% to 10.4%, as depicted in Table S2, which might effectively promote catalytic combustion of acrylonitrile.

XPS of O1s and Cu $2p_{3/2}$ for $LaFe_{0.8}Cu_{0.2}O_3$, $LaCo_{0.8}Cu_{0.2}O_3$, and $LaMn_{0.8}Cu_{0.2}O_3$ samples are profiled in Fig. S3a and S3b with the related quantitative analyses being simultaneously conducted in Section S7 of Surface element study in SI. The surface components of atomic La, M (M=Fe, Co, Mn, Cu), and O derived from XPS are listed in Table S3. It can be found that $LaFe_{0.8}Cu_{0.2}O_3$ possessed the comparatively low contents of surface atomic Cu (2.06%) but presented the highest Cu^{2+}/Cu^{+} ratio. This result suggests that Fe-O-Cu structure is inclined to expose high valence of Cu. On one hand, $LaFe_{0.8}Cu_{0.2}O_3$ provided the lowest O_{ads}/O_{lat} atomic ratio (1.31) among the Cu-doped samples which might benefit for inhibiting the excessive oxidation of nitrogen atom into the higher N-valence products like N_2O, NO, and NO_2. On the other hand, the O_{ads}/O_{lat} of $LaFe_{0.8}Cu_{0.2}O_3$ (1.31) is much higher than that of $LaFeO_3$ (0.67), which is mainly due to the increase of oxygen vacancy due to Cu substitution. The high density of anionic oxygen vacancy on $LaFe_{0.8}Cu_{0.2}O_3$ was believed to be favorable for the adsorption and activation of O_2 [30], and hence enhancing catalytic activity for acrylonitrile combustion.

3.2. Activity test

The temperature dependence on the conversion of acrylonitrile as well as the yields of N-containing products (N_2, NH_3, N_2O, NO, NO_2) and C-containing products (CO_2, CO) during nitrile combustion over $LaFeO_3$ and $LaB_{0.8}Cu_{0.2}O_3$ (B=Fe, Co, and Mn) samples are depicted in Fig. 1a–d. As presenting in Fig. 1a, the initial activity is achieved at 200 °C for pure $LaFeO_3$ perovskite and at 150 °C for Cu-doped samples. acrylonitrile conversion occurring over pure $LaFeO_3$ is gradually increased upon temperature and reach 100% at 400 °C; however, Cu substitution could prompt the temperature reduce to 250 °C for a complete acrylonitrile conversion and the Co- and Mn-based perovskite doped by Cu can also achieve this effect. It demonstrates that the perovskite-type materials commonly show excellent activities for catalytic removal of acrylonitrile even at low temperatures. Apart from acrylonitrile conversion being a crucial indicator for evaluating the combustion performances, N_2 and CO_2 yields constituting other criterions are also important due to the possible releasing of toxic byproducts (NH_3, NO, N_2O, NO_2, and CO) during acrylonitrile combustion. As shown in Fig. 1a, N_2 yield of $LaFe_{0.8}Cu_{0.2}O_3$ is apparently higher than those of the other samples at temperatures above 300 °C (around 80%). It has been found that an enhancement in N_2 yield at T < 400 °C for $LaFe_{0.8}Cu_{0.2}O_3$ was likely caused by Cu^{2+} substitution improve its redox ability at

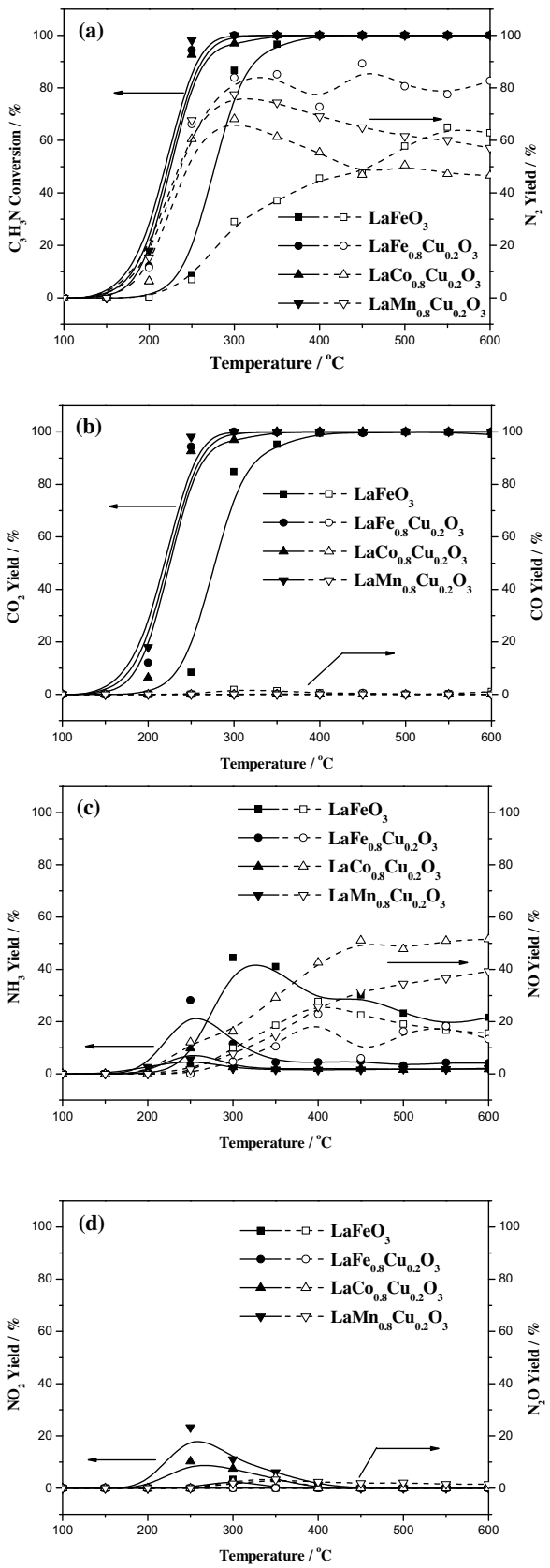

Fig. 1. Catalytic performance as a function of temperature during acrylonitrile combustion over $LaFeO_3$ and $LaB_{0.8}Cu_{0.2}O_3$ (B=Fe, Co, and Mn) samples: (a) acrylonitrile conversion and N_2 yield; (b) CO_2 and CO yield; (c) NH_3 and NO yield; (d) N_2O and NO_2 yield. Conditions: 3000 ppm AN, 1.6 vol% O_2, and GHSV = 120,000 h^{-1}.

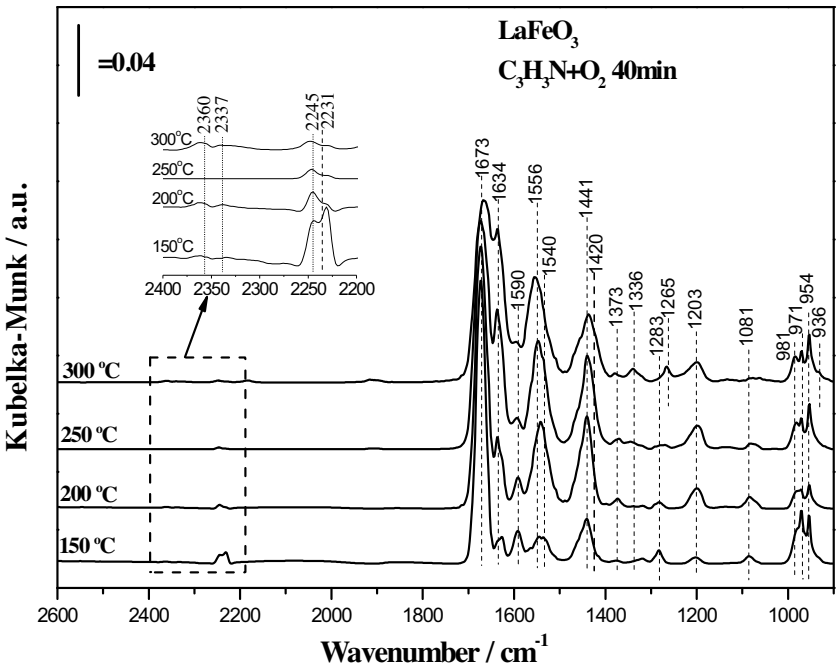

Fig. 2. DRIFT spectra of $LaFeO_3$ with an exposure to 1.2 vol% acrylonitrile, 6.4 vol% O_2, with He to be the balance gas in the range of 150–300 °C.

low temperatures. The existence of Fe—O—Cu structure in the lattice of perovskite could benefit to generate N_2 in the SCR of NO reaction, which was demonstrated by the previous reports [18,22]. While at the high temperatures from 400 °C to 600 °C, the oxidation property of Fe becomes weaker than those of Mn and Co, according to H_2-TPR results, which leads $LaFe_{0.8}Cu_{0.2}O_3$ to produce more N_2 as well as $LaMn_{0.8}Cu_{0.2}O_3$ and $LaCo_{0.8}Cu_{0.2}O_3$ to produce large amount of undesirable NO_x byproducts. The profiles of CO_2 and CO yields depicted in Fig. 1b show that carbonaceous species, in the presence of excessive O_2, are directly oxidized to CO_2 over these three samples, which indicates that CO_2 generation is only related to O_2 concentration and hardly affected by perovskite compositions. The yields of N-containing byproducts (NH_3 and NO) and (N_2O and NO_2) are respectively illustrated in Fig. 1c and d, which are helpful to understand the trails of nitrogen except generating N_2. As seen from Fig. 1c and d, NH_3 and N_2O with relatively lower N valences are usually yielded at low temperatures from 150 to 400 °C, associated with an order of $LaFe_{0.8}Cu_{0.2}O_3 > LaCo_{0.8}Cu_{0.2}O_3 > LaMn_{0.8}Cu_{0.2}O_3$ for NH_3 yield and an order of $LaMn_{0.8}Cu_{0.2}O_3 > LaCo_{0.8}Cu_{0.2}O_3 > LaFe_{0.8}Cu_{0.2}O_3$ for N_2O yield. This finding indicates that mechanism for acrylonitrile catalytic combustion over these samples may vary from one to another. For $LaFe_{0.8}Cu_{0.2}O_3$ sample, due to the large generation of N_2 accompanying with certain amount of NH_3, it is speculated that NH_3 is an important intermediate during the reaction. Based on above analyses, it is realized that $LaFe_{0.8}Cu_{0.2}O_3$ not only possessing higher acrylonitrile activity but also exhibiting the best selectivity toward N_2 and CO_2 is a promising candidate as a catalyst for acrylonitrile selective combustion.

3.3. Mechanism study based on DRIFTS

The mechanism of catalytic combustion of acrylonitrile over different types of catalyst has been investigated [2,3,7]. Basically, two main mechanisms can be distinguished: hydrolysis mechanism in which acylamino (—$CONH_2$) was formed through nitrile (—CN) hydrolysis over Fe/SBA-15 and oxidation mechanism in which the isocyanate (-NCO) could be generated over Cu/SBA-15 through an oxidation of nitrile (—CN) [5,31]. Nanba et al. [7] also demonstrated that acrylonitrile was mostly converted to isocyanate (—NCO) over Cu/ZSM-5, indicating that it tends to follow oxidation mechanism in the presence of copper species. However, the acrylonitrile catalytic combustion reaction mechanism over perovskites has so far not been studied.

3.3.1. In-situ *DRIFTs of catalytic combustion of acrylonitrile over $LaFeO_3$*

$LaFeO_3$ perovskite shows certain reactivity for acrylonitrile combustion, while Cu substitution ($LaFe_{0.8}Cu_{0.2}O_3$) not only lowers the temperature for acrylonitrile complete conversion by 100 °C but also greatly improves the N_2 yield up to 80% at high temperature (above 300 °C). In order to sufficiently understand the surface reaction mechanism influenced by Cu substitution, the related mechanisms conducting over $LaFeO_3$ and $LaFe_{0.8}Cu_{0.2}O_3$ perovskites are investigated via *in-situ* DRIFTS study conducted at different temperatures. The contradistinction of acrylonitrile catalytic conversion between these two samples was explored with an emphasis on the formation of diverse intermediates due to Cu substitution. Fig. 2 shows IR spectra during an exposure of $LaFeO_3$ perovskite to gas mixture containing 1.2 vol.% acrylonitrile, 6.4 vol.% O_2, with He balance gas in a temperature range of 150–300 °C. Each curve depicts a change of surface species after reactant gas is fed at corresponding temperatures for 40 min. The band at 971 cm^{-1} attributed to bending vibration of C—H of gaseous acrylonitrile is clearly observed. Additionally, the bands at 2231 and 2245 cm^{-1} were also detected at 150 °C attributed to the C≡N functional group in acrylonitrile, implying that acrylonitrile was adsorbed upon $LaFeO_3$ through N-terminal adsorption. The adsorption process is described as Eq. (1), in which solid line represents a coordinate or ionic bond (respectively for adspecies or perovskite):

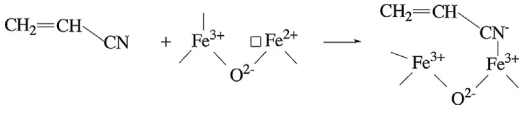

(1)

The intensity of these peaks was significantly reduced along with the rise of temperature. At T = 300 °C, only small amounts

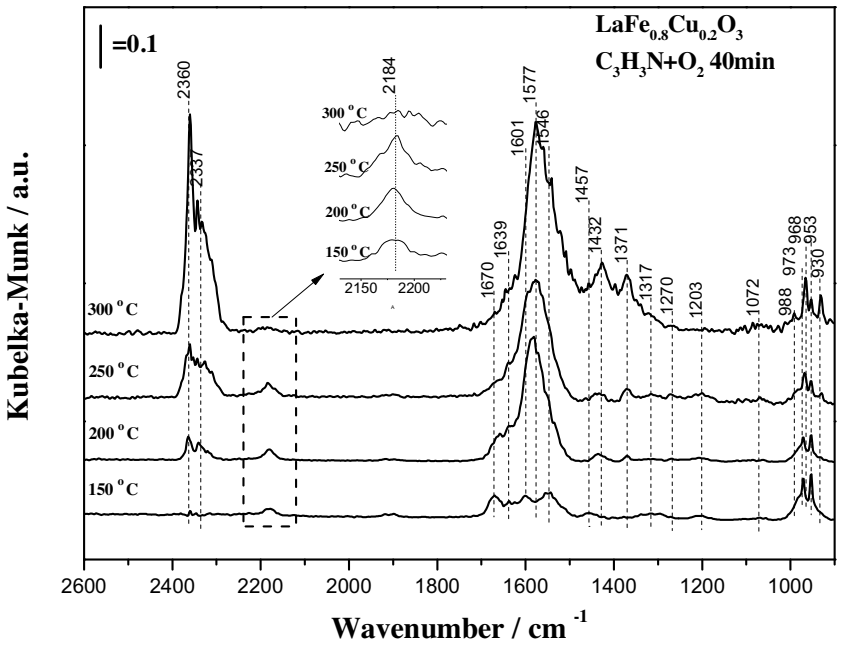

Fig. 3. DRIFT spectra of $LaFe_{0.8}Cu_{0.2}O_3$ with an exposure to 1.2 vol% acrylonitrile, 6.4 vol% O_2, with He to be the balance gas in the range of 150–300 °C.

of —CN groups are remained, suggesting that —CN fragment was mostly converted into other species upon the increasing temperature. According to the literature reports [2,7], the bands exhibited at 1203, 1540, 1590, and 1673 cm^{-1} were assigned to the adsorbed acrylamide species, among which the band at 1673 cm^{-1} represented the C=C vibrations [ν(C=C)] of acrylamide and the weak bands at 1203 and 1590 cm^{-1} correspond to the asymmetric deformation of NH_3 [$\delta_{as}(NH_3)$] coordinated to Lewis acid sites [32,33]. Besides, the synergy of N—H bending vibration and C-N stretching vibration generates a small band at 1540 cm^{-1}. All the evidences strongly demonstrated that acrylonitrile was easily hydrolyzed to generate acrylamide over Fe-based catalyst at relatively low temperatures, as formulated by Eq. (2):

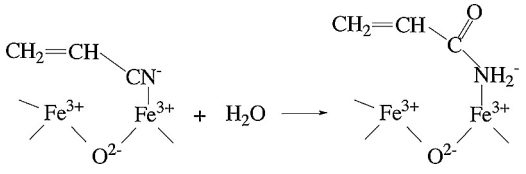

(2)

Simultaneously, the bands at 1081, 1373, 1441, 1556, and 1634 cm^{-1} were also detected and attributed to acrylic acid species produced by the further hydrolysis of adsorbed acrylamide species according to the literature [2,34]. The bands at 1441 and 1540 cm^{-1} were assigned to $\nu_{as}(COO^-)$ and $\nu_s(COO^-)$ of acetate species, respectively [8,35,36]. Furthermore, the band at 1373 cm^{-1} due to δ(C—H) and the one at 1081 cm^{-1} due to ν_s(C—O) provided additional evidences for the existence of acrylic acid [37]. It is noted that acrylic acid species was detectable even at 150 °C, in spite of its quantity being very rare. At the elevated temperatures, the characteristic bands of acrylic acid became more apparent while that of acrylamide declined slightly; convincingly showing that acrylic acid was obtained through further hydrolysis of acrylamide. Meanwhile, the characteristics of bending bands [δ(N—H)] of acrylamide were detected at 954 and 981 cm^{-1} associated with a shoulder at 936 cm^{-1} attributed to gaseous NH_3 [38]. The transformation from acrylamide to acrylic acid and ammonia can be described by Eqs. (3) and (4):

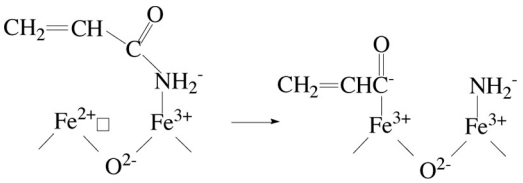

(3)

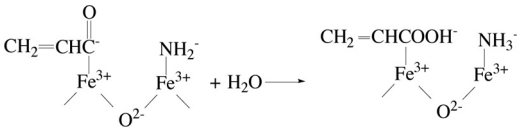

(4)

Furthermore, the weak band of 1283 cm^{-1} appearing at 150 °C was also observed and attributed to the linear nitrite [22], but retained its lower quantity which is consistent with the results obtained from activity test. It is worth noting that the band of linear nitrite shifted lightly toward lower wavenumber of 1265 cm^{-1} at 300 °C due to a formation of more stable chelating nitrite instead of the linear one [39]. This indicates that molecular vibration of nitrite has been reinforced, to some extent, making nitrite more stable. Two additional bands at 1336 and 1420 cm^{-1} could be detected which was respectively attributed to the bridging nitrite and ionic nitrate [$Fe^{3+}(NO_3^-)_3$] species. Subsequently, the characteristic band attributed to $\nu_{as}(COO^-)$ at 300 °C showed a blue shift from 1540 cm^{-1} to 1556 cm^{-1} due to a synergistic effect between acetate and nitrate [38,40]. These results indicate that NH_3 or $-NH_2$ species could be oxidized to adsorbed NO^- at relatively high temperatures which is further oxidized to unstable nitrite species, subsequently to more stable nitrate species. The process can be described by Eqs. (5) and (6). However, the intensity of these NO_x^-

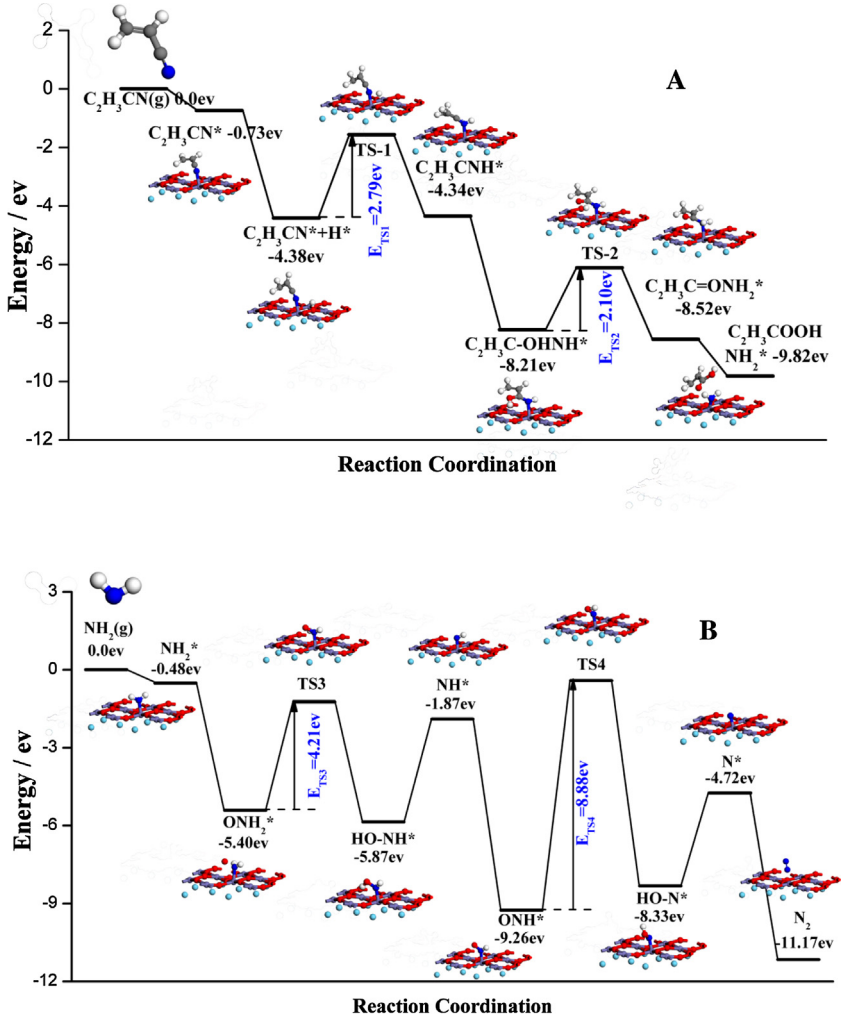

Fig. 4. A, B: Gibbs free energy profile for the reaction to generate acrylic acid and N_2 on $LaFeO_3$.

species with high oxidation states were never significant, indicating the low yields of possible N_2O, NO, and NO_2 products.

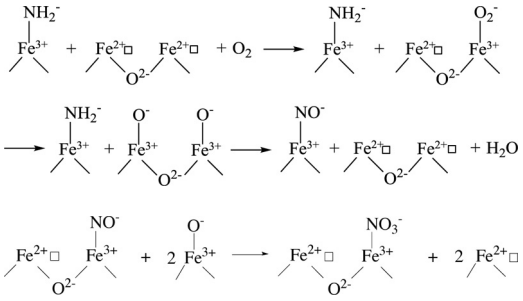

(5)

(6)

On the basis of above analysis, it gives sufficient explanation for the higher NH_3 amount as compared to NO_x amount achieved over $LaFeO_3$ perovskite. It was previously reported that acrylonitrile decomposition over Cu-ZSM-5 proceeds by a hydrolysis of nitrogen-containing intermediates, such as —NCO [7]. However, the noticeable —NCO band was never observed, showing that the formation of —NCO species is impossible as well as its hydrolysis to form NH_3 and further oxidation to yield N_2 unlikely occur on the bare $LaFeO_3$ perovskite. Accordingly, it is concluded that NH_3 or $-NH_2$ was further oxidized at active sites by surface oxygen and two NH_x species were thereafter combined to generate azo-species with the cleavage of N-H bond.

3.3.2. In-situ *DRIFTS of catalytic combustion of acrylonitrile over* $LaFe_{0.8}Cu_{0.2}O_3$

In the case of $LaFe_{0.8}Cu_{0.2}O_3$ and exposure under 150 °C, the bands at 1203, 1546, 1601, and 1670 cm^{-1} (see Fig. 3) are attributed to the adsorbed acrylamide species, indicating that Cu corporation into $LaFeO_3$ has some influences on the generation of intermediate species during acrylonitrile catalytic elimination, among which the band at 1670 cm^{-1} was accordingly attributed the C=C vibrations [ν(C=C)] of acrylamide. Besides, the band at 1639 cm^{-1} was ascribed to C=O stretching vibration [ν_s(C=O)], and the bands at 1072, 1432, and 1546 cm^{-1} belong to ν_s(C—O), $\nu_s(COO^-)$, and $\nu_{as}(COO^-)$ of carboxylic acid species, respectively. However, these characteristic bands are herein not significant especially for C=C vibrations [ν(C=C)] at 1670 cm^{-1}. In comparison of Fig. 2 with Fig. 3, it is noted that the characteristic band of C=C vibrations [ν(C=C)] was clearly detected in the case of $LaFeO_3$ sample between 150 and 300 °C but became minor for $LaFe_{0.8}Cu_{0.2}O_3$, indicating that the oxidation of anomeric carbon is very weak for $LaFeO_3$ sample and the existence of C=C is unstable in the presence of Cu because Cu doping promotes the surface oxidation ability at low temperatures. Furthermore, characteristic bands of acrylamide species were not obvious on the surface of $LaFe_{0.8}Cu_{0.2}O_3$ at 150 °C as compared with those of $LaFeO_3$, illustrating that acrylamide was not stable and nitrile is likely to be oxidized on $LaFe_{0.8}Cu_{0.2}O_3$.

As shown in Fig. 3, C=C vibration [ν(C=C)] at 1670 cm^{-1} is not only apparently observed with an increase of temperature, which

display a fast reaction to form carboxylic acid (-COOH). This oxidation process is described as Eq. (7).

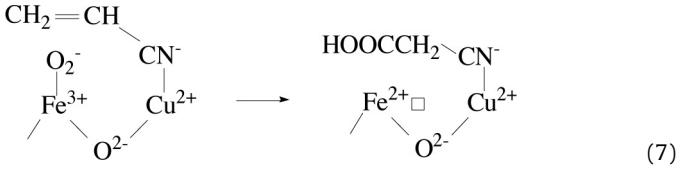

(7)

Surprisingly, a sharp new band occurring at 1577 cm^{-1} was detected when the temperature rose to 200 °C. According to the literature reports [41], this band fits perfectly with the adsorbed malonate species, which shows strong vibrations at 1577 cm^{-1} [$\nu_{as}(COO^-)$] and 1432 cm^{-1} $\nu_s[(COO^-)]$. The latter band consists of contributions from the symmetric stretch vibrations of carboxylate groups and C—H bending modes. This demonstrates that anomeric carbon was simultaneously oxidized to obtain carboxylic acid species, in addition to N-containing group being oxidized. It is the most notable contrast between $LaFeO_3$ and $LaFe_{0.8}Cu_{0.2}O_3$ for the corresponding combustion behaviors. N_2 generation could be accomplished via an interaction of two —NH species subsequent with a dehydrogenation process, while the formation of malonate species is described by Eq. (8):

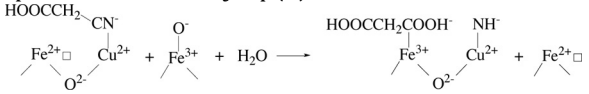

(8)

Furthermore, the infrared bands of malonic acid species have become more apparent, and prove the stable existence of malonic acid species at the range of 200–300 °C. The band at 1317 cm^{-1} could be attributed to the monodentate carbonate and its intensity gradually increased accompanying with the rising temperatures. In addition, the IR bands attributed to bending vibration of ν_δ(C—H) were noticed at 953 and 988 cm^{-1}. In contrast to the findings on $LaFeO_3$ sample, a new low-intensity band appeared at 2184 cm^{-1}, owing to surface isocyanide (NCO) species [5,40]. Raskó and Kiss previously investigated the adsorption and catalytic reactions of acetonitrile over TiO_2-supported rhodium catalysts knowing that CH_3CN could be first dissociated into CN and successively oxidized into the surface isocyanide (NCO) species [5,42]. Whereas, Liu et al. held another point that nitrates and oxygenates take part in the reaction to form —NCO species [43]. Besides, researchers offer diverse views on the consequent reaction of NCO species. In the case of the SCR of NO_x by C_2H_5OH or C_3H_6 over Cu/Al_2O_3 or Ag/Al_2O_3, He et al. proposed that NCO reacts with NO + O_2 and even nitrates to yield N_2 [34,36,37,40], while the NCO species was rather stable over $Cu/Ti_{0.7}Zr_{0.3}O_2$ catalyst in an atmosphere of NO + O_2 [43,44] and then it might be hydrolyzed to form NH_3 and successively reacted with nitrate/nitrite to yield N_2. In this study, NCO species were observed 2184 cm^{-1} and the band intensity increased monotonously as temperature rises, but suddenly decreased at 300 °C. Moreover, an interesting phenomenon could be noted that the bands at 930 and 960 cm^{-1} attributed to gaseous NH_3 became significant once the characteristic band of NCO decreased, implying that the pathway of NCO hydrolysis to form NH_3 is more credible. The formation of isocyanide and further hydrolysis are described by Eqs. (9) and (10):

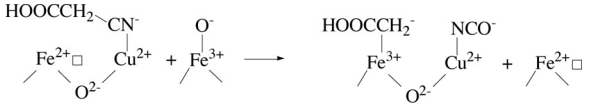

(9)

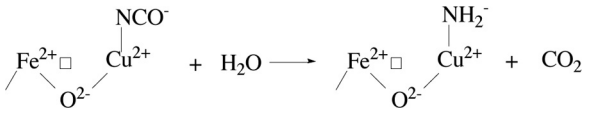

(10)

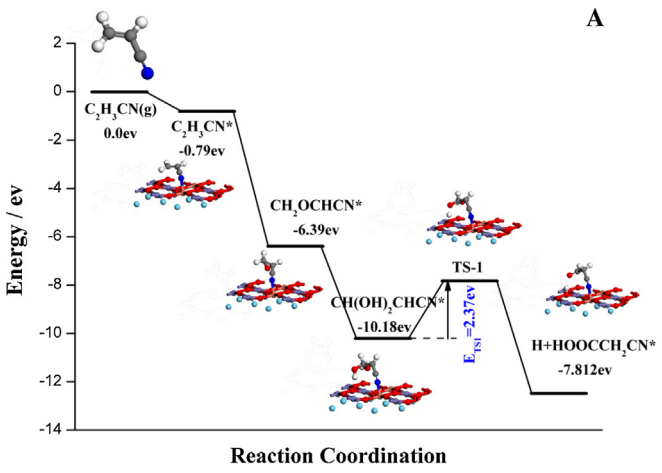

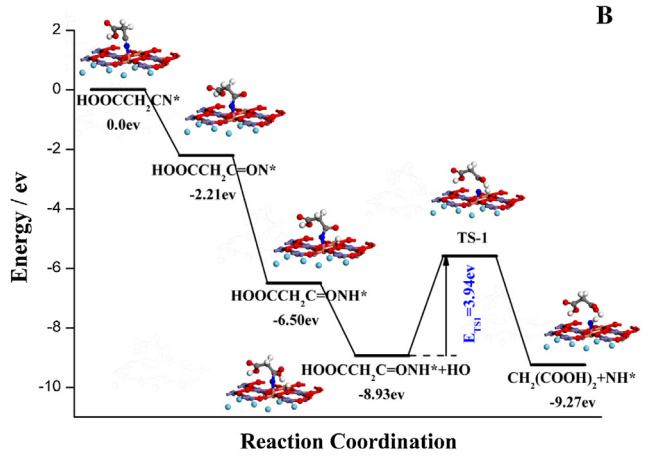

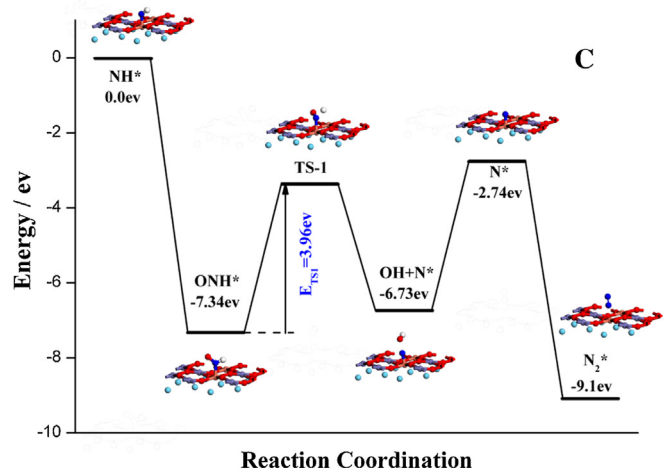

Fig. 5. A, B, C: Gibbs free energy profile for the reaction to generate $HOOCCH_2CN$-Fe, malonic acid species, and N_2 on $LaFe_{0.8}Cu_{0.2}O_3$.

In addition to malonate, small amount of NCO species thought as an intermediate was obtained over $LaFe_{0.8}Cu_{0.2}O_3$, which implies a mechanism obviously different from that related to $LaFeO_3$. However, the intensity of NCO was just minor compared with that of malonate, so the process of NCO hydrolysis might be a side reaction. The bands at 2263, 2337 cm^{-1} were attributed to gaseous CO_2 and the intensity of these two bands gradually increased from 150 to 300 °C. It is known that the formed malonic acid species

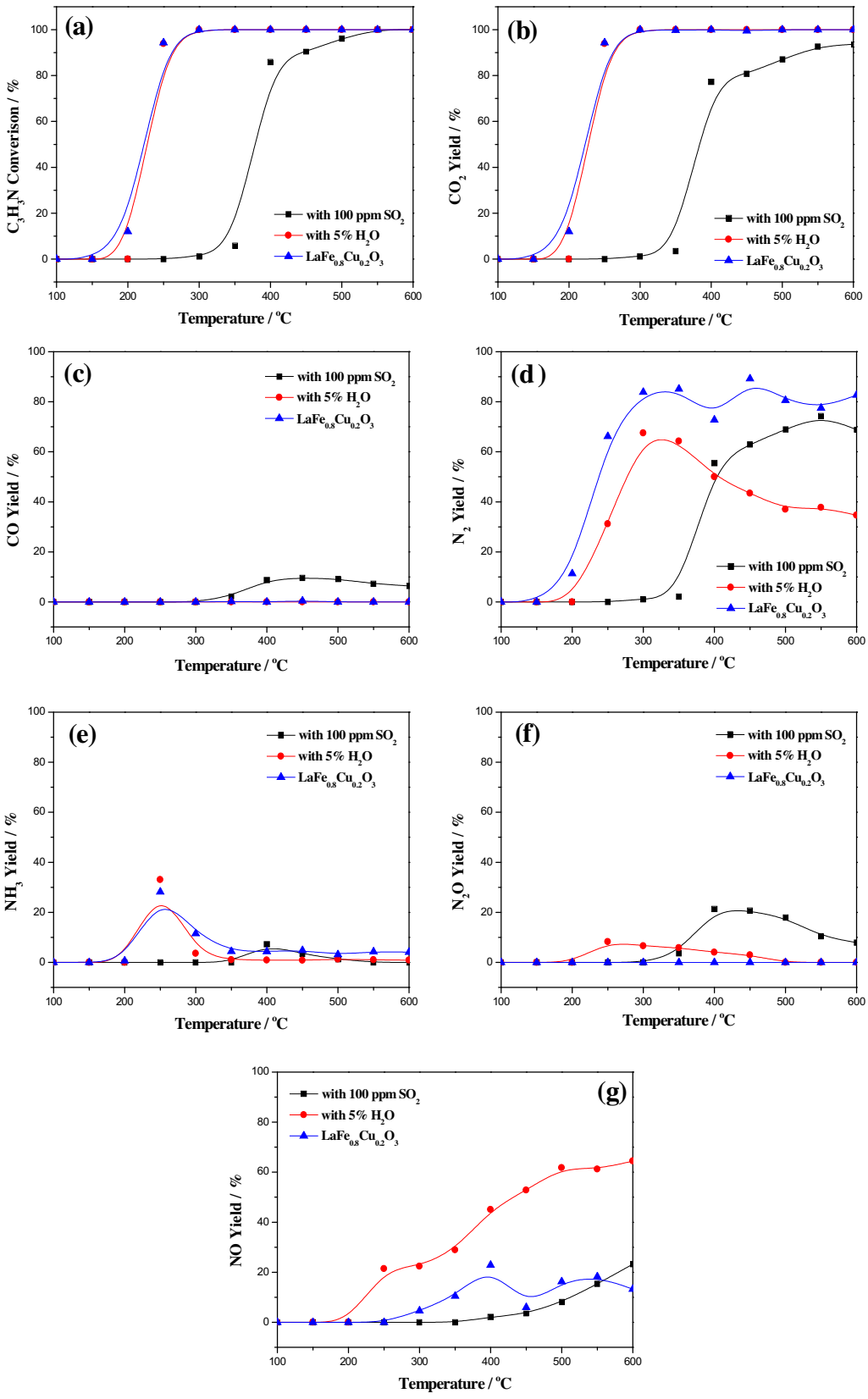

Fig. 6. The water and sulfur resistance over $LaFe_{0.8}Cu_{0.2}O_3$ at the whole temperature range: (a) C_3H_3N conversion, (b) CO_2 yield, (c) CO yield, (d) N_2 yield, (e) NH_3 yield, (f) N_2O yield, (g) NO_x yield.

was finally oxidized into CO_2 at the elevated temperatures [36,45]. The weak bands at 1203 and 1601 cm^{-1} could be attributed to the coordinated NH_3 on Lewis acid sites [32]. The band appearing at 1203 cm^{-1} for $LaFeO_3$ sample was intensified along with the temperature increase, but there is little information at 1203 cm^{-1} for $LaFe_{0.8}Cu_{0.2}O_3$, suggesting NH_3 generation over $LaFeO_3$ is more

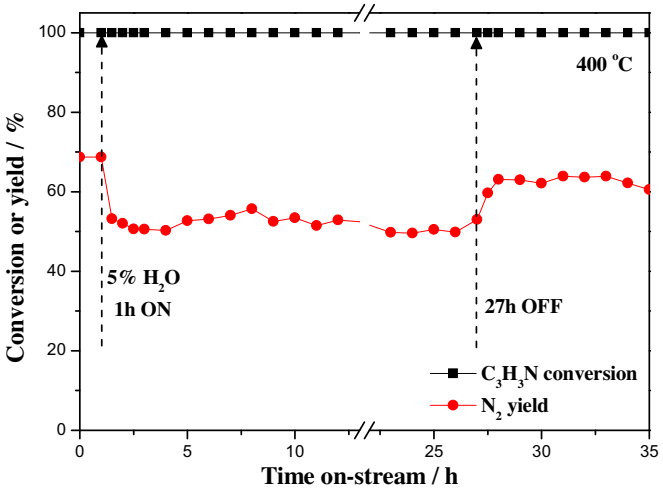

Fig. 7. The H_2O resistance stability over $LaFe_{0.8}Cu_{0.2}O_3$ with change of time.

easily than that over $LaFe_{0.8}Cu_{0.2}O_3$ at 300 °C. This result is consistent with that obtained from activity measurement. In addition, the bands at 1457 and 1546 cm^{-1} assigned to $\nu_s(COO^-)$ and $\nu_{as}(COO^-)$ of carboxylate species were detected again, which explained that the partial oxidation reaction occurred at 150 °C over Cu-doped perovskite. With the temperature rises, a red shift from 1457 to 1432 cm^{-1} together with an overlapping of band at 1546 cm^{-1} with that at 1577 cm^{-1} indicated that abundant carboxylate species were formed. It is worth noting that the area of carboxylate characteristic band achieving at 200–300 °C was larger than that achieving at 150 °C, which seems to demonstrate carboxylate was generated not only at N-end but also at C-end. Likewise, the very weak band of 1270 cm^{-1} achieving at 250 and 300 °C attributed to the chelating nitrite species was also observed [37].

In general, Cu substitution could efficiently improve the transformation of anomeric carbon into carboxylate. Besides, some NCO species were also partly generated at N-end in addition to acrylamide formation. Subsequently, the consumption of the N-containing species including the NCO could be mainly caused by the reaction with H_2O, which was considered as two crucial steps to generate N_2.

3.4. Mechanism study based on DFT calculation

In order to further verify how acrylonitrile was adsorbed on the surface of Fe-based perovskite, how the intermediate species was formed, and how the final products, especially N_2, was generated during the reaction, DFT calculation was introduced combined with *in-situ* IR results, aiming at giving a more elaborative reaction mechanism.

The possible adsorption modes and adsorption energies were calculated based on the FeO-terminated $LaFeO_3$ because B-site cations are commonly regarded as active centers for the perovskite-type oxides. Acrylonitrile adsorption is illustrated in Section S8 of SI. The calculated adsorption configurations and energies are shown in Fig. S4 and Table S4. In light with DFT calculation, it is proposed that configure A is the most-likely configuration for the adsorbed acrylonitrile existing over $LaFeO_3$ in a manner described by Eq. (1) with an adsorption energy of −0.73 ev.

3.4.1. Formation of acrylic acid over $LaFeO_3$

To further confirm the generation of acrylic species as evidenced by *in-situ* infrared study, the free energies of the possible intermediates and transition states as well as the reaction pathways were calculated. The results on the Gibbs-free-energy profiles are displayed in Fig. 4A.

As shown in Fig. 4A, acrylonitrile was initially adsorbed on the surface of $LaFeO_3$ with formation of Fe^{3+}-NC structure. Subsequently, Fe^{3+}-NC was attacked by H atom from the adsorbed H_2O considering that the reaction process followed a hydrolysis mechanism. Surprisingly, H atom was steadily adsorbed at O-site adjacent to Fe-site, with E_{ads} = −3.46 ev. It should surmount an energy barrier of 2.79 ev to obtain $C_2H_3CNH^-$-Fe^{3+} species accompanying with an activation of N-terminal species, as formulated by Eq. (11). Additionally, triple bonds of —CN were partly fractured to form —CN- along with a change in bond length from 1.187 to 1.244 Å. And then, attempt to conduct a hydroxylation of $C_2H_3C{=}NH^-$-Fe^{3+} species from adsorbed hydroxyl has been done, finding that —OH was connected with C atom adjacent to N-terminal forming a $C_2H_3C{-}OHNH^-$-Fe^{3+} structure, which is described by Eq. (12). Due to the unstable existence of this structure, H atom of hydroxyl was subsequently transferred to N atom with an energy barrier of 2.79 ev, generating the relatively stable structure of acrylamide ($C_2H_3C{=}ONH_2^-$-Fe^{3+}), in accordance with the formulation by Eq. (2). C=N bond was continually destroyed and the bond length was also stretched to 1.418 Å with forming the C—N single bond which is not stable anymore. Subsequently, this C—N single bond was broken quickly to form unsaturated structure which reacted with the hydroxyl from gas phase to yield acrylic species. Ultimately, acrylic acid was desorbed from the surface of catalyst and subsequently adsorbed upon the other active sites (as depicted by Eq. (3)). The $-NH_2$ species were still adsorbed at the active sites steadily and further oxidized into N_2.

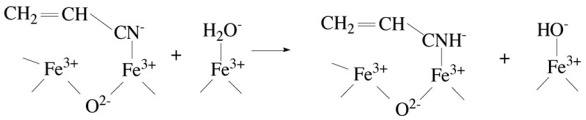

(11)

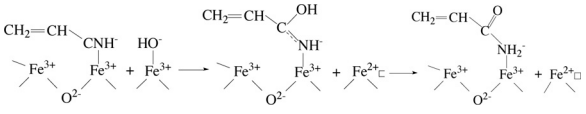

(12)

3.4.2. Formation of target product of N_2

As shown in Fig. 4B, $-NH_2$ species was initially adsorbed on the surface of catalyst with energy of 0.48 ev and then reacted with atomic O^- to get ONH_2^--Fe^{3+} species, associated with E_{ads} = −5.39 ev. Subsequently, these species quickly undergo hydrogen redistribution that H atom was connected to N atom linked with O atom, forming $HO{-}NH^-$-Fe^{3+} species. This process should overcome an energy barrier of 4.21 ev. The hydroxyl was immediately desorbed from surface leaving NH^--Fe^{3+} species on the surface. Subsequently, another atomic O^- reacted with N atom achieving O^-NH-Fe^{3+} species, conquering a high energy barrier of 8.88 ev to obtain $HO{-}N^-$-Fe^{3+} species. Finally, the N^--Fe^{3+} interacted with another N atom to get the end product of N_2 after hydroxyl was stripped. In the process of N_2 generation, the rate-determining step is N—H bond cleavage accompanied with O—H bond connection. Moreover, NH_3 generation is relatively simple that only interaction with H atom from H_2O dissociation could form NH_3. This explains the easy generation of a large number of gaseous NH_3 over $LaFeO_3$ sample during the activity test. The process of oxidation from $-NH_2$ species to N_2 are described in Eqs. (13)–(15).

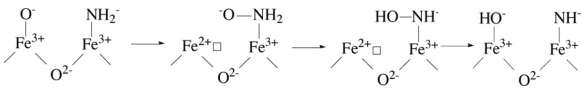

(13)

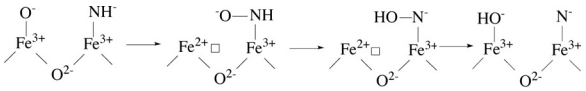

(14)

Table 1
Bands observed on $LaFeO_3$ and $LaFe_{0.8}Cu_{0.2}O_3$ catalyst during *in-situ* DRIFTS experiments and corresponding surface species and vibrations to which they were assigned.

Samples	Category	Peak location (cm^{-1})	Surface species	Vibration	Reference
$LaFeO_3$	C-containing	971	Ethenyl	δ(C—H)	
		1673	Ethylene	ν(C=C)	
		1540, 1441	Acetate	$\nu_{as}(COO^-)$, $\nu_s(COO^-)$	[8,39,40]
		1373	Methyl	$\delta(-CH_3)$	[41]
		1081	Carboxylic acid	ν_s(C—O)	[41]
	N-containing	2231, 2245	Nitrile	ν(C≡N)	
		954, 981	Acrylamide	δ_s(N—H)	[35]
		1203, 1590	Ammonia	$\delta_{as}(NH_3)$	[36,37]
		1283	Linear nitrite		[22]
		1265	Chelating nitrite		[42]
		1420	Bridging nitrite		
		1336	Ionic nitrate		
$LaFe_{0.8}Cu_{0.2}O_3$	C-containing	1670	Ethylene	ν(C=C)	
		1639, 1072, 1432, 1546	Carboxylic acid	ν_s(C=O), $\nu_s(COO^-)$, $\nu_s(COO^-)$, ν_{as}(C—O)	
		1577, 1371, 1432, 1317	Malonate	$\nu_{as}(COO^-)$ $\nu_s(COO^-)$	[45]
		953, 988	Monodentate carbonate	ν_δ(C—H)	
	N-containing	2184	Isocyanide (NCO)		[5,43]
		1270	Chelating nitrite		[42]

ν: stretching; δ: bending; s: symmetric, as: asymmetric.

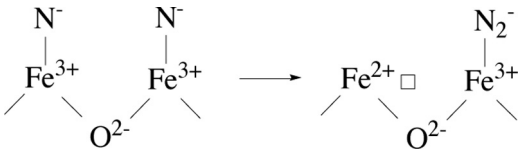
(15)

3.4.3. The mechanism occurring over $LaFe_{0.8}Cu_{0.2}O_3$ distinct from that occurring over $LaFeO_3$

Because there are significant differences on the generated intermediate species in *in-situ* DRIFTS experiments for $LaFeO_3$ and $LaFe_{0.8}Cu_{0.2}O_3$, the DFT simulation was further used to explore the diversity in details and explain the promoting effect of Cu doping into perovskite on N_2 yield. The related discussion of acrylonitrile adsorption is illustrated in Section S9 of SI and the optimized geometry structures including bond lengths of Fe-O and Cu-O for $LaFe_{0.8}Cu_{0.2}O_3$ as well as the calculated energies of acrylonitrile adsorption are listed in Table S5.

Since anomeric carbon has been proved to generate carboxylate easily according to *in-situ* infrared experiments, we have to initially make sure how anomeric carbon was oxidized to carboxylate before N-terminal oxidation was considered. As shown in Fig. 5A, acrylonitrile molecule was also adsorbed on the surface of $LaFe_{0.8}Cu_{0.2}O_3$ with formation of Cu^{2+}-NC structure. In order to get the carboxylate, atomic oxygen (O^-) from adsorbed molecule oxygen (O_2^-) cleaving the carbon–carbon double bonds was adsorbed at C—C site with E_{ads} = −5.90 ev with a H atom connected with another atomic oxygen to form hydroxyl. Moreover, anomeric carbon was attacked by hydroxyl and adsorbed it steadily. Furthermore, H atom from C-site is restructured at O atom forming another hydroxyl. Due to the electronic influence of oxygen, two hydroxyl groups upon a carbon atom are essentially unstable. H atom of hydroxyl was cleavaged from O atom with an energy barrier of 2.37 ev, generating the relatively stable structure $HOOCCH_2CN$—Cu. This process is described by Eq. (16) and (17).

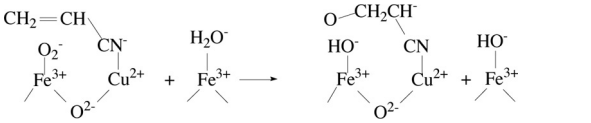
(16)

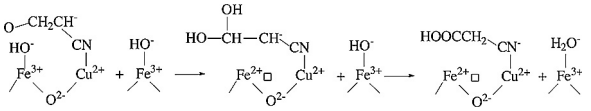
(17)

atomic O^- was used to attack Cu^{2+}-CN^- showing that it was adsorbed steadily on C-site, forming C=O double bond. In a similar way, two O atoms were drawn close to nitrile and anomeric carbon. However, it is found that one O atom was adsorbed at N-site and another one stably existed at adjacent Cu-site. The difference paths of adsorbed acrylonitrile reacting with oxygen between $LaFeO_3$ and $LaFe_{0.8}Cu_{0.2}O_3$ were illustrated in Fig. 5B. Obviously, the ability for carbonaceous species oxidation of $LaFe_{0.8}Cu_{0.2}O_3$ is better than that of $LaFeO_3$. This is because the bond length of Fe-O have been shortened resulting in increasing of oxygen density around Fe-site. The improvement of surface oxygen adsorption can be proposed through the generation of anionic vacancies in the crystal lattice by Cu incorporation, giving an easier oxygen diffusion from the bulk to the surface [12]. Fig. 5B presents the formation process of important intermediate species malonic acid species and NH with surmounting an energy barrier of 3.94 ev. This process is described by Eqs. (18) and (19).

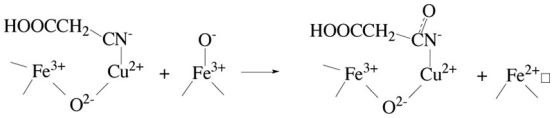
(18)

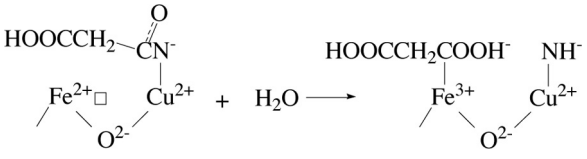
(19)

Furthermore, Fig. 5C depicted the process of N_2 generation. It should overcome an energy barrier of 3.96 ev to obtain N^* at $LaFe_{0.8}Cu_{0.2}O_3$, which is much lower than the value for $LaFeO_3$. The process is described by Eqs. (20) and (21).

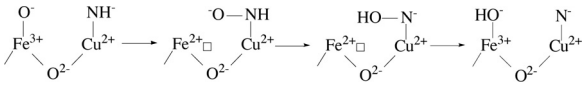
(20)

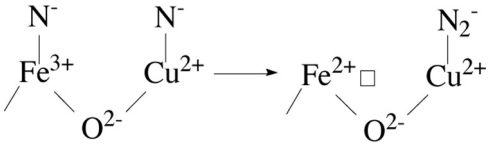
(21)

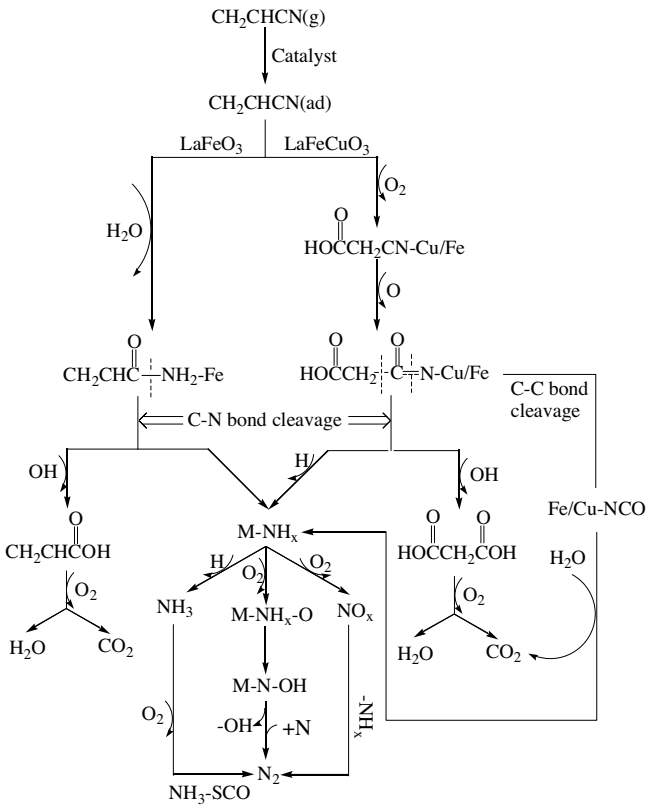

Scheme 1. Reaction network for proposed mechanism of the acrylonitrile catalytic combustion reaction over the $LaFeO_3$ and $LaFe_{0.8}Cu_{0.2}O_3$ samples.

3.4.4. *Reaction network for the mechanism of catalytic combustion of acrylonitrile over $LaFeO_3$ and $LaFe_{0.8}Cu_{0.2}O_3$*

The DFT calculations provide sufficient and favorable supporting information for the role of the acrylic acid and malonic acid species respectively forming over $LaFeO_3$ and $LaFe_{0.8}Cu_{0.2}O_3$. On the basis of the *In-situ* DRIFTS study and DFT calculation, an overall mechanism of the catalytic combustion of acrylonitrile for $LaFeO_3$ and $LaFe_{0.8}Cu_{0.2}O_3$ is proposed. The main intermediates (appearing in Table 1) are depicted in reaction network of Scheme 1. Acrylonitrile is firstly adsorbed at active sites of $LaFeO_3$ or $LaFe_{0.8}Cu_{0.2}O_3$, while two distinct mechanisms to yield N_2 are verified due to their different chemical features. It follows hydrolysis-dominating mechanism on the surface of $LaFeO_3$, in which the adsorbed acrylonitrile is hydrolyzed into acrylamide and C—N bond is further broken to gain acrylic acid and —NH_2 species. Acrylic acid is subsequently oxidized to H_2O and CO_2. Simultaneously, —NH_2 is oxidized to final product N_2. In the process of N_2 generation, the rate-determining step is the adsorbed O captured H atom from —NH_2 to form hydroxyl (—OH). In contrast, it follows oxidation-dominating mechanism over $LaFe_{0.8}Cu_{0.2}O_3$, in which C-end is initially oxidized into carboxylic acid species and C atom adjacent to N is also oxidized. Next, the formation of N_2 over $LaFe_{0.8}Cu_{0.2}O_3$ is attributed to two separate pathways: (i) the C—N bond cleavage occurred, in which the crucial intermediate of malonic acid species and —NH species are acquired and (ii) C—C bond is fractured to generate small amount of —NCO species. Subsequently, malonic acid species is thereafter oxidized to H_2O and CO_2, and —NH/-NH_2 is transferred into final product N_2. In addition, —NCO species can also react with H_2O to yield CO_2 and —NH_2 species. It is worth noting that in the process of N_2 generation for $LaFe_{0.8}Cu_{0.2}O_3$ sample the rate-determining step is N—H bond fracture and O—H connection again. The presence of Cu can greatly reduce the energy barrier for the transformation from —NH—O to —N—OH, as verified by theoretical calculation, and thus promote the improvement of N_2 yield.

Table 2
Adsorption species and site, adsorption energy, and bond lengths involved in single molecule adsorption and influence of H_2O or SO_2 pre-adsorption for reactants and products adsorption on $LaFe_{0.8}Cu_{0.2}O_3$.

Species	sites	E_{ads} (ev)	Bond lengths (Å)
C_2H_3CN	Cu – site	−0.842	d_{Cu-N} = 1.87
O_2	Fe – site	−1.859	d_{Fe-O} = 1.76
N_2	Fe – site	−0.031	d_{Fe-N} = 3.58
NO	Cu – site	−1.188	d_{Cu-N} = 1.83
SO_2	Fe – site	−0.419	d_{Fe-O} = 1.96
H_2O	Fe – site	−0.430	d_{Fe-O} = 2.18
H_2O pre-adsorbed C_2H_3CN	Cu – site	−0.814	d_{Cu-N} = 2.09, d_{Fe-O} = 2.05
H_2O pre-adsorbed O_2	Fe – site	−1.944	d_{Cu-O} = 2.09, d_{Fe-O} = 1.76
H_2O pre-adsorbed N_2	Fe – site	−0.086	d_{Cu-O} = 2.14, d_{Fe-N} = 3.86
H_2O pre-adsorbed NO	Fe – site	−0.769	d_{Cu-N} = 2.05, d_{Fe-O} = 1.85
SO_2 pre-adsorbed C_2H_3CN	Cu – site	−0.435	d_{Cu-N} = 2.02, d_{Fe-O} = 1.83

3.5. *Resistance to water vapor and sulfur dioxide poisonings*

According to the catalytic activities of acrylonitrile (C_2H_3CN) combustion exhibiting in Fig. 1, $LaFe_{0.8}Cu_{0.2}O_3$ sample was verified to be the optimal catalyst. In order to understand the performance of the catalyst under the real tail-gases conditions, the effect of H_2O and SO_2 on catalytic behaviors during the temperature range of 100–600 °C was investigated. Fig. 6a shows the acrylonitrile conversion at the presence of 5% H_2O or 100 ppm SO_2. Fig. 6b and c present the corresponding yields of C-containing products (CO_2 and CO), and Fig. 6d–g show the yields of N-containing products (N_2, NH_3, N_2O, and NO). As depicted in Fig. 6a, a slightly deactivation of acrylonitrile conversion accompanying with 5% steam addition into the feed at low temperatures (100–300 °C) and a serious drop along with 100 ppm SO_2 introduction at the whole temperature region were observed. The formation of CO_2 product was hardly affected by the presence of H_2O; however, a distinct decline in N_2 yield at 300–600 °C was noticed as well as NO yield was significantly improved due to H_2O deactivation. In the presence of 100 ppm SO_2, the decrease of yield of the targeted N_2 was likely ascribed to a decline in number of active centers via coverage by adsorbed sulfurous species (SO_2, SO_3, SO_3^{2-}, SO_4^{2-}).

SO_2 poisoning mechanism over perovskite was pointed out by several authors [17,46] that competitive adsorption of SO_2 with reactants as well as the coverage of active sites by surface sulfite and sulfate species may lead to the severe decline of catalytic activity. In our case, the pre-adsorption of SO_2 can lead to a decrease of energy of acrylonitrile adsorption, with a value of −0.435 ev being essentially higher than that of its adsorption alone (−0.842 ev), indicating that acrylonitrile adsorption may be greatly suppressed by SO_2 pre-adsorption. In addition, SO_3 and SO_4^{2-} species formed during the oxidation process are more stable than SO_2. Combustion activity in the presence of SO_2 was thus inhibited due to a worse acrylonitrile adsorption based on above reasons. In contrast, water adsorption merely resulted in a moderate deactivation. As shown in Table 2, the adsorption energy of H_2O at Cu-top site is −0.430 ev, whereas the adsorption energy of O_2 and acrylonitrile are −1.859 ev and −0.842 ev, respectively, indicating that adsorbed H_2O was less stable than the adsorbed O_2 and C_2H_3CN molecules. Furthermore, the bond strength of acrylonitrile adsorption was slightly weakened after H_2O pre-adsorption. Similar to SO_2 poisoning, the diminution in the number of adsorption sites available for O_2 resulted from H_2O competitive adsorption should also reduce the surface oxidation ability. However, NO yield was improved in the presence of H_2O which is likely to be associated with a “NO formation” mecha-

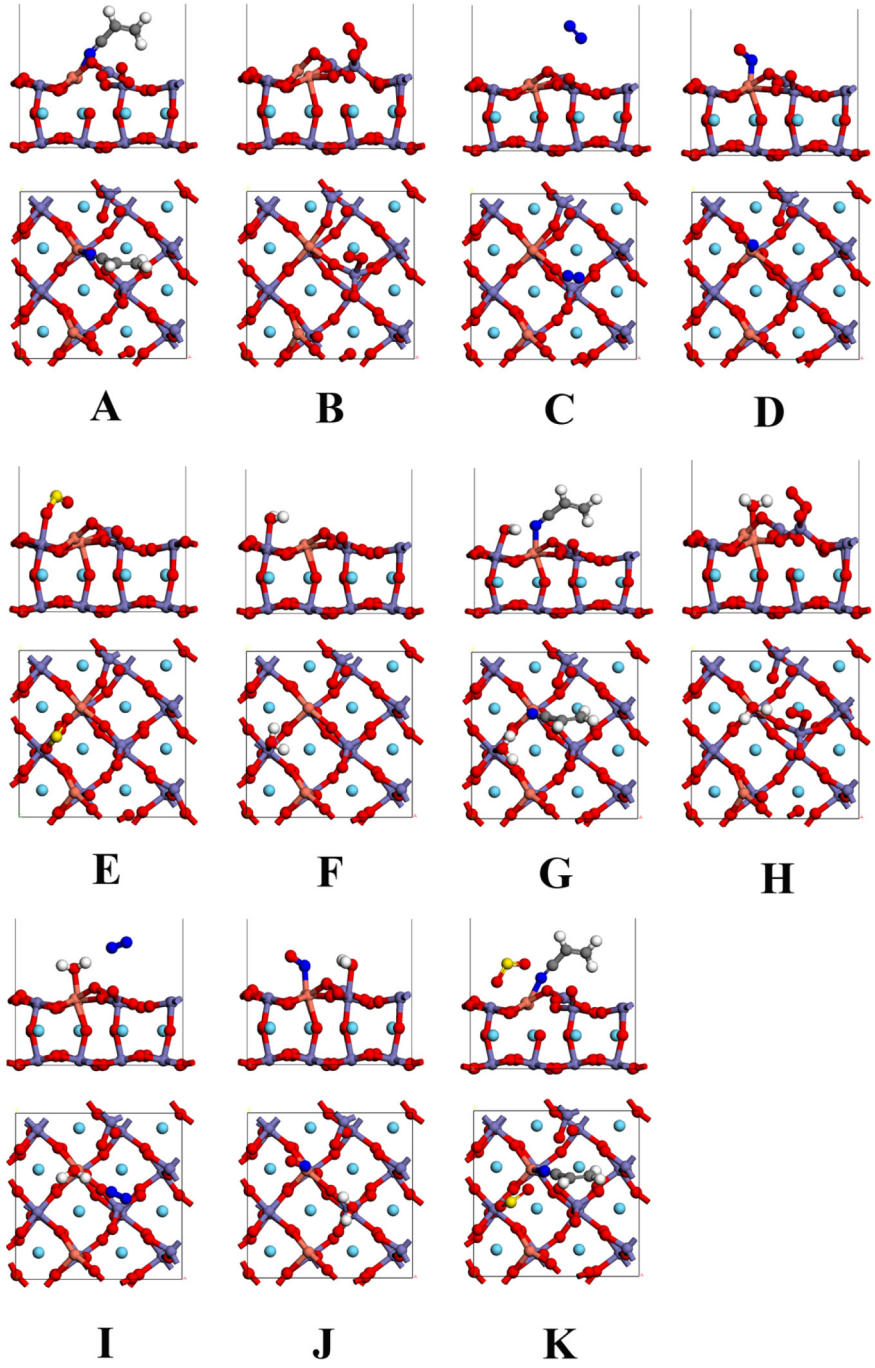

Fig. 8. Side and top view of optimized geometries involved in single molecule adsorption and influence of H_2O or SO_2 pre-adsorption for reactants and products adsorption on $LaFe_{0.8}Cu_{0.2}O_3$: (A) C_2H_3CN, (B) O_2, (C) N_2, (D) NO, (E) SO_2, (F) H_2O, (G) $H_2O + C_2H_3CN$, (H) $H_2O + O_2$, (I) $H_2O + N_2$, (J) H_2O + NO, (K) $SO_2 + C_2H_3CN$.

nism. According to the previous study [47], the adsorption of H_2O may follow Eqs. (22) and (23):

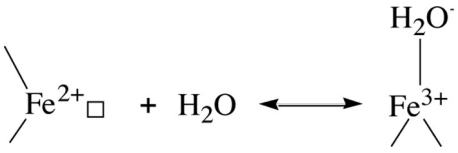

(22)

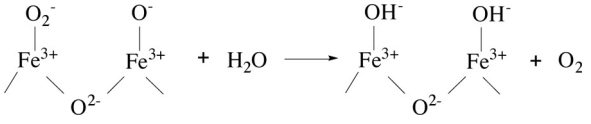

(23)

The adsorption of water can cause an increase of surface hydroxyl. According to Fig. 5C , it would across an energy barrier of 3.96 ev to form adsorbed atomic N. In contrast, it was seen that —ONH could dehydrogenate H atom to obtain the adsorbed NO species. Thereafter, the adjacent hydroxyl capture H atom from —ONH to obtain H_2O molecule by surmounting 1.37 ev (Eq. (24)) which is less than that of forming adsorbed N atom, indicating that the $LaFe_{0.8}Cu_{0.2}O_3$ surface with high hydroxyl coverage is inclined to acquire H atom generating adsorbed NO. Furthermore, we compared the desorption ability between adsorbed NO with adsorbed H_2O. As shown in Table 2, the adsorption energy of individual NO at Fe-site is −1.188 ev while H_2O pre-adsorption can make this value increased up to −0.769 ev, showing that the $LaFe_{0.8}Cu_{0.2}O_3$ surface

with H_2O adsorption may have stronger NO desorption ability. Furthermore, the N_2 adsorption energy was reduced from −0.031 ev to −0.086 ev due to H_2O pre-adsorption. This might be the reason that N_2 yield declines obviously with 5% H_2O addition.

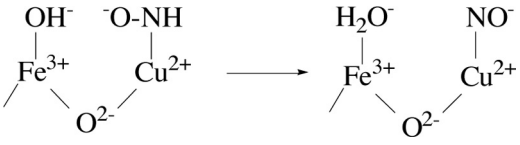

(24)

The reversibility of H_2O deactivation was studied by adding 5% H_2O vapor after the reaction system was stable at 400 °C for 1 h and subsequently removing H_2O at 27 h from the reactant stream as depicted in Fig. 7. All the optimized geometries involved in single molecule adsorption and influence of H_2O or SO_2 pre-adsorption for the related adsorption of reactants and products on LaFe0.8Cu0.2O_3 are shown in Fig. 8. The activity of acrylonitrile was marginally affected by the presence of H_2O, but about 50–70% decrease of N_2 yield occurred. Fortunately, this deactivation caused by H_2O addition can be well recovered by removing steam from the feed. This result shows that the presence of H_2O does not permanently poison the perovskite with its structure being unchanged in the presence of moisture. Consequently, this reversible deactivation caused by H_2O addition is believed to involve the existence of hydroxyl favorable for capturing H atom from —ONH species.

4. Conclusion

In this study, a series of perovskite catalysts with different B-site transition-metals partially substituted by Cu were systematically investigated for the selective catalytic combustion of acrylonitrile, among which $LaFe_{0.8}Cu_{0.2}O_3$ not only showed the excellent acrylonitrile conversion activity but also presented the best yield towards N_2 being a promising candidate used as a catalyst for selective acrylonitrile → N_2 oxidation. It has been found that Cu-substitution could effectively enhance the redox capacity at low temperatures due to easy Cu^{2+} to Cu^0 reduction for the perovskite samples and increase the relative concentration of surface adsorption oxygen, which is beneficial for the improvement of acrylonitrile activity at low temperatures. This result suggests that the ability of oxygen adsorption is promoted at $LaFe_{0.8}Cu_{0.2}O_3$ surface which is attributed to the generation of anionic vacancies in the crystal lattice by Cu incorporation. Furthermore, *In-situ* DRIFTS investigations combined with DFT calculations were used to elaborately analyze the catalytic mechanism for acrylonitrile combustion, revealing two distinct mechanisms occurred: hydrolysis-dominate mechanism in which the acrylic species steadily existed at the surface of $LaFeO_3$ and oxidation-dominating mechanism for $LaFe_{0.8}Cu_{0.2}O_3$ in which the crucial intermediate of malonic acid species was acquired. Additionally, Cu substitution into $LaFeO_3$ could greatly reduce energy barrier for the transformation from —NH—O to —N—OH, which is the rate-determining step from —NH_x species to N atom, and further promote the improvement of N_2 yield. In addition, $LaFe_{0.8}Cu_{0.2}O_3$ represented satisfactory resistance to water vapor poisoning.

Appendix A. Supplementary data

Supplementary data associated with this article can be found, in the online version, at http://dx.doi.org/10.1016/j.apcatb.2016.05.025.

References

[1] A. Gervasini, G. Vezzoli, V. Ragaini, Catal. Today 29 (1996) 449–455.
[2] T. Nanba, S. Masukawa, J. Uchisawa, A. Obuchi, J. Catal. 259 (2008) 250–259.
[3] T. Nanba, S. Masukawa, J. Uchisawa, A. Obuchi, Appl. Catal. A 419–420 (2012) 49–52.
[4] I.O.Y. Liu, N.W. Cant, J. Catal. 195 (2000) 352–359.
[5] R. Zhang, D. Shi, N. Liu, Y. Cao, B. Chen, Appl. Catal. B 146 (2014) 79–93.
[6] T. Nanba, S. Masukawa, A. Ogata, J. Uchisawa, A. Obuchi, Appl. Catal. B 61 (2005) 288–296.
[7] T. Nanba, S. Masukawa, J. Uchisawa, A. Obuchi, J. Mol. Catal. A 276 (2007) 130–136.
[8] F. Poignant, J.L. Freysz, M. Daturi, J. Saussey, Catal. Today 70 (2001) 197–211.
[9] S. Royer, D. Duprez, F. Can, X. Courtois, C. Batiot-Dupeyrat, S. Laassiri, H. Alamdari, Chem. Rev. 114 (2014) 10292–10368.
[10] M.A. Pena, J.L.G. Fierro, Chem. Rev. 101 (2001) 1981–2017.
[11] S. Royer, D. Duprez, ChemCatChem 3 (2011) 24–65.
[12] W. Yang, R. Zhang, B. Chen, N. Bion, D. Duprez, S. Royer, J. Catal. 295 (2012) 45–58.
[13] X. Yan, Q. Huang, B. Li, X. Xu, Y. Chen, S. Zhu, S. Shen, J. Ind. Eng. Chem. 19 (2013) 561–565.
[14] S. Royer, H. Alamdari, D. Duprez, S. Kaliaguine, Appl. Catal. B 58 (2005) 273–288.
[15] V. Blasin-Aubé, J. Belkouch, L. Monceaux, Appl. Catal. B 43 (2003) 175–186.
[16] W.B. Li, J.X. Wang, H. Gong, Catal. Today 148 (2009) 81–87.
[17] R. Zhang, H. Alamdari, S. Kaliaguine, Appl. Catal. A 340 (2008) 140–151.
[18] R. Zhang, A. Villanueva, H. Alamdari, S. Kaliaguine, J. Catal. 237 (2006) 368–380.
[19] R. Zhang, A. Villanueva, H. Alamdari, Kaliaguine. Appl. Catal. A 307 (2006) 85–97.
[20] R. Zhang, A. Villanueva, H. Alamdari, S. Kaliaguine, Appl. Catal. B 64 (2006) 220–233.
[21] R. Zhang, W. Yang, N. Luo, P. Li, Z. Lei, B. Chen, Appl. Catal. B 146 (2014) 94–104.
[22] W. Yang, R. Zhang, B. Chen, D. Duprez, S. Royer, Environ. Sci. Technol. 46 (2012) 11280–11288.
[23] L.A. Isupova, A.A. Budneva, E.A. Paukshtis, V.A. Sadykov, J. Mol. Catal. A 158 (2000) 275–280.
[24] L. Sun, J. Hu, H. Qin, M. Zhao, K. Fan, J. Phys. Chem. C 115 (2011) 5593–5598.
[25] X. Liu, J. Hu, B. Cheng, H. Qin, M. Zhao, C. Yang, Sensor Actuat. B 139 (2009) 520–526.
[26] X. Liu, B. Cheng, J. Hu, H. Qin, Comp. Mater. Sci. 68 (2013) 90–94.
[27] G. Henkelman, B.P. Uberuaga, H. Jonsson, J. Chem. Phys. 113 (2000) 9901–9904.
[28] L. Zhang, Y. Zhang, H. Dai, J. Deng, L. Wei, H. He, Catal. Today 153 (2010) 143–149.
[29] P. Xiao, L. Zhong, J. Zhu, J. Hong, J. Li, H. Li, Y. Zhu, Catal. Today 258 (2015) 660–667.
[30] G. Bai, H. Dai, J. Deng, Y. Liu, F. Wang, Z. Zhao, W. Qiu, C.T. Au, Appl. Catal. A 450 (2013) 42–49.
[31] R. Zhang, D. Shi, N. Liu, B. Chen, L. Wu, L. Wu, W. Yang, Catal. Today 258 (2015) 17–27.
[32] Z. Wu, B. Jiang, Y. Liu, H. Wang, R. Jin, Environ. Sci. Technol. 41 (2007) 5812–5817.
[33] R. Zhang, N. Luo, W. Yang, N. Liu, B. Chen, J. Mol. Catal. A 371 (2013) 86–93.
[34] Y. Yu, X. Zhang, H. He, Appl. Catal. B 75 (2007) 298–302.
[35] F. Zhang, S. Zhang, N. Guan, E. Schreier, M. Richter, R. Eckelt, R. Fricke, Appl. Catal. B 73 (2007) 209–219.
[36] Y. Yu, H. He, Q. Feng, J. Phys. Chem. B 107 (2003) 13090–13092.
[37] Y. Yu, H. He, Q. Feng, H. Gao, X. Yang, Appl. Catal. B 49 (2004) 159–171.
[38] N. Bion, J. Saussey, M. Haneda, M. Daturi, J. Catal. 217 (2003) 47–58.
[39] L. Liu, Y. Chen, L. Dong, J. Zhu, H. Wan, B. Liu, B. Zhao, H. Zhu, K. Sun, L. Dong, Y. Chen, Appl. Catal. B 90 (2009) 105–114.
[40] H. He, C. Zhang, Y. Yu, Catal. Today 90 (2004) 191–197.
[41] P. Borer, S.J. Hug, J. Colloid Interf. Sci. 416 (2014) 44–53.
[42] J. Raskó, J. Kiss, Appl. Catal. A 303 (2006) 56–61.
[43] J. Liu, X. Li, Q. Zhao, C. Hao, D. Zhang, Environ. Sci. Technol. 47 (2013) 4528–4535.
[44] J. Liu, X. Li, Q. Zhao, C. Hao, S. Wang, M. Tadé, ACS Catal. 4 (2014) 2426–2436.
[45] M.Z. Hossain, Y. Yuan, A.S. Teja, J. Supercrit. Fluid. 95 (2014) 457–461.
[46] M. Alifanti, R. Auer, J. Kirchnerova, F. Thyrion, P. Grange, B. Delmon, Appl. Catal. B 41 (2003) 71–81.
[47] R. Zhang, H. Alamdari, S. Kaliaguine, Appl. Catal. B 72 (2007) 331–341.